The Astrophysical Journal, 683:137–148, 2008 August 10

MILKY WAY MASS MODELS AND MOND

Stacy S. McGaugh
Department of Astronomy, University of Maryland, College Park, MD 20742-2421; ssm@astro.umd.edu
Received 2008 March 12; accepted 2008 April 8

ABSTRACT

Using the Tuorla-Heidelberg model for the mass distribution of the Milky Way, I determine the rotation curve predicted by MOND (modified Newtonian dynamics). The result is in good agreement with the observed terminal velocities interior to the solar radius and with estimates of the Galaxy's rotation curve exterior thereto. There are no fit parameters: given the mass distribution, MOND provides a good match to the rotation curve. The Tuorla-Heidelberg model does allow for a variety of exponential scale lengths; MOND prefers short scale lengths in the range 2.0 kpc $\lesssim R_d \lesssim$ 2.5 kpc. The favored value of R_d depends somewhat on the choice of interpolation function. There is some preference for the "simple" interpolation function as found by Famaey & Binney. I introduce an interpolation function that shares the advantages of the simple function on galaxy scales while having a much smaller impact in the solar system. I also solve the inverse problem, inferring the surface mass density distribution of the Milky Way from the terminal velocities. The result is a Galaxy with "bumps and wiggles" in both its luminosity profile and rotation curve that are reminiscent of those frequently observed in external galaxies.

Subject headings: dark matter — galaxies: kinematics and dynamics — galaxies: spiral

Online material: color figures

1. INTRODUCTION

A persistently viable alternative to dark matter is the modified Newtonian dynamics (MOND) of Milgrom (1983a, 1983b, 1983c). MOND is known to perform well in fitting the rotation curves of individual galaxies (e.g., Begeman et al. 1991; Sanders 1996; de Blok & McGaugh 1998; Sanders & Verheijen 1998; Sanders & McGaugh 2002; Sanders & Noordermeer 2007), possessing a predictive power well beyond that available from mass models with a mix of luminous and dark mass. On the other hand, MOND fares less well on the larger scales of clusters of galaxies (e.g., Sanders 2003; Pointecouteau & Silk 2005; Clowe et al. 2006; Angus et al. 2007, 2008), seeming to require more mass than currently observed in known baryonic forms. This is a genuine problem, but also a partial success as Milgrom (1983c) was among the first to note the potential mass of the intracluster medium. Clusters are not without their puzzles in the context of dark matter (Hayashi & White 2006; McCarthy et al. 2007; Springel & Farrar 2007; Milosavljević et al. 2007; Milgrom & Sanders 2008; Angus & McGaugh 2008; Nusser 2008; Broadhurst & Barkana 2008). This is an oft-repeated theme; systems that pose problems for MOND often make little sense in terms of dark matter either. On the positive side, MOND performs well in a greater variety of systems than seems to be widely appreciated (Bekenstein 2006; McGaugh 2006; Milgrom 2008). For example, it correctly describes (Milgrom 2007; Gentile et al. 2007) the behavior of tidal dwarfs (Bournaud et al. 2007), which pose an existential challenge to cold dark matter (CDM). We should therefore be cautious of an eagerness to dismiss the idea entirely on the basis of one type of object, or the natural distrust of the unfamiliar, and rather seek as many precision tests as possible.

As a modified force law, MOND makes strong and testable predictions. In the absence of invisible mass, the observed kinematics of an object in the MOND regime of low acceleration should follow from its observed mass distribution just as planetary motions follow from purely Newton dynamics in the solar system. One galaxy that we are intimately familiar with is our own Milky Way, for which a wealth of high-quality data are available.

Famaey & Binney (2005) investigated MOND in the Milky Way in the context of the Basel model (Bissantz & Gerhard 2002; Bissantz et al. 2003). Since that time, the number and quality of observational constraints has continued to improve. Moreover, the gas mass is not negligible in MOND, being nearly 20% of the total. Here I consider this in the context of the Milky Way for the first time.

The goal of this paper is to use one type of observation to predict another. Given the mass distribution of the Milky Way, does MOND predict a plausible rotation curve consistent with the available data? Inverting the question, can the mass distribution be inferred from the kinematic data? The point is not to find the best fit involving every possible kind of data (see Widrow et al. 2008 for such an exercise in the conventional context). Rather, I seek to use one type of datum to *predict* an entirely independent set of observations.

The paper is organized as follows. In § 2 I describe MOND as applied here, considering a variety of interpolation functions. In § 3 I describe the mass distribution of the Milky Way, adopting the Tuorla-Heidelberg model (Flynn et al. 2006) for the stellar mass distribution and utilizing the tabulation of Olling & Merrifield (2001) for the gas distribution. In § 4 I present the results of applying MOND to the adopted mass model. In § 5 I invert the question and infer the deviations from a smooth exponential luminosity profile implied by the "bumps and wiggles" in the terminal velocity curve. The conclusions are summarized in § 6.

2. MOND AND THE INTERPOLATION FUNCTION

The basic idea of MOND (Milgrom 1983a) is that rather than invoking dark matter to explain mass discrepancies in extragalactic systems, one modifies the force law such that

$$\boldsymbol{g}_{\rm N} = \mu(x)\boldsymbol{a}, \tag{1}$$

where $\boldsymbol{g}_{\rm N}$ is the acceleration calculated using Newtonian dynamics, and $\boldsymbol{a}$ is the actual resulting acceleration. The modification occurs not at some length scale, but at the acceleration scale a_0, with $x = a/a_0$ (here $a = |\boldsymbol{a}|$). The interpolation function $\mu(x)$

has the property $\mu \rightarrow 1$ in the limit of large accelerations $a \gg a_0$ so that Newtonian behavior is recovered. In the limit of small accelerations the modification applies, with $\mu \rightarrow x$ for $a \ll a_0$.

The acceleration scale a_0 is very small. Begeman et al. (1991) found $a_0 = 1.2 \times 10^{-10}$ m s^{-2} $= 3700$ km^2 s^{-2} kpc^{-1} from fits to high-quality rotation curves. More recently, Bottema et al. (2002) estimated $a_0 = 3000$ km^2 s^{-2} kpc^{-1} and McGaugh (2004) $a_0 \approx 4000$ km^2 s^{-2} kpc^{-1}, the latter utilizing population synthesis estimates of the stellar mass. Here I adopt the intermediate Begeman et al. (1991) value and keep a_0 fixed while considering different possible interpolation functions. The reader should bear in mind that in addition to the uncertainty in a_0 reflected in the variety of determinations, the best-fit value is likely to depend somewhat on the choice of interpolation function.

As noted by Milgrom (1983a) and Felten (1984), equation (1) does not conserve momentum. This was addressed by Bekenstein & Milgrom (1984), who wrote the modified Poisson equation

$$\nabla \cdot \left[\mu\left(\frac{|\nabla\Phi|}{a_0}\right)\nabla\Phi \right] = 4\pi G\rho. \tag{2}$$

This form of modified gravity obeys the conservation laws. Milgrom (1994, 1999) also provides a conservative albeit nonlocal formalism for modified inertia rather than modified gravity.

Application of equation (1) has been highly successful in fitting rotation curves. It is exact for circular orbits in the modified inertia theory. For modified gravity as it applies in spiral galaxies, equation (1) is an approximation to equation (2) that is usually correct to $\sim$15% (Brada & Milgrom 1995). For our considerations here this suffices; it is not necessary to invoke the aquadratic Lagrangian theory of Bekenstein & Milgrom (1984), much less the generally covariant theories of Bekenstein (2004) or Sanders (2005).

Indeed, for our purposes here, we merely need the empirically proven formula connecting surface density and rotation velocity (McGaugh 2004). MOND is formulated in terms of the actual acceleration, as appropriate for a dynamical theory. However, in the Milky Way we have a better handle on the surface densities that predict the Newtonian acceleration. Therefore, it is convenient to make the substitution $\nu(y) = \mu^{-1}(x)$, where $y = g_{\rm N}/a_0$. While not appropriate as the basis for a theory, this is functionally equivalent when using the empirical approximation of equation (1). Replacing $\mu(x)$ with $\nu^{-1}(y)$ has the advantage that $g_{\rm N}(R)$ can be directly computed from $\Sigma(R)$ with purely Newtonian dynamics. Assuming circular motion ($a = V_c^2/R$), we then have

$$V_c^2 = \nu(y)V_b^2, \tag{3}$$

where V_b is the Newtonian rotation velocity expected for the baryons. The Newtonian velocity V_b and acceleration $g_{\rm N}$ are computed for appropriate mass distributions (see § 3): no simplifying assumption like a "spherical disk" is made. Moreover, the right-hand side of equation (3) depends only on surface density, making it possible to predict the rotation curve without reference to it through $x = V_c^2/(a_0R)$.

Rotation curve fitting has traditionally employed the interpolation function (Milgrom 1983b; Sanders & McGaugh 2002)

$$\mu_2(x) = \frac{x}{\sqrt{1+x^2}}. \tag{4}$$

This form is not specified by any deeper theory, and other forms are possible. From habitual use equation (4) has come to be called the "standard" interpolation function.

More recently, it has been suggested that the "simple" function

$$\mu_1(x) = \frac{x}{1+x} \tag{5}$$

may give a better description of some data (Famaey & Binney 2005; Zhao & Famaey 2006; Sanders & Noordermeer 2007). Both this and the standard function are part of the family

$$\mu_n(x) = x(1+x^n)^{-1/n}. \tag{6}$$

If we make the transformation $\mu \rightarrow \nu^{-1}$, we find the corresponding family

$$\nu_n(y) = \left(\frac{1}{2} + \frac{1}{2}\sqrt{1+4y^{-n}}\right)^{1/n}. \tag{7}$$

Milgrom & Sanders (2008) have suggested other possible families. One is

$$\tilde{\nu}_n(y) = \frac{1}{\sqrt{1-e^{-y}}} + ne^{-y}, \tag{8}$$

with another being

$$\bar{\nu}_n(y) = [1-\exp(-y^n)]^{-1/2n} + \left(1-\frac{1}{2n}\right)\exp(-y^n). \tag{9}$$

These forms may have some virtue in causing artifacts that appear as rings of dark matter (Milgrom & Sanders 2008) such as that described by Jee et al. (2007). Note that $\nu(y)$ is effectively the same as the mass discrepancy $D(y)$ defined by McGaugh (2004), but I make the distinction that D is an empirical quantity while ν is a construct of MOND.

The simple function (eq. [5]) appears to have some important virtues in the transition from Newtonian to MOND regimes (Famaey & Binney 2005; Sanders & Noordermeer 2007). However, it may have difficulties with solar system tests (Sereno & Jetzer 2006; Wallin et al. 2007; Iorio 2007). This occurs because of a rather gradual approach to the Newtonian regime. Interestingly, it is just right (Milgrom 2006; McCulloch 2007) for explaining the *Pioneer* anomaly (Anderson et al. 1998). Note that this implies a conflict in the data. The *Pioneer* anomaly is quite accurately measured, but may not be a dynamical effect, so it remains unclear which interpretation to prefer.

It is possible to have an interpolation function that retains the virtues of the simple function on galaxy scales ($\sim a_0$) while having no impact in the inner solar system ($\sim 10^8 a_0$). One possible family is

$$\hat{\nu}_n(y) = \left[1-\exp\left(-y^{n/2}\right)\right]^{-1/n} \tag{10}$$

such that

$$\hat{\nu}_1(y) = \left(1-e^{-\sqrt{y}}\right)^{-1}, \tag{11a}$$

$$\hat{\nu}_2(y) = \left(1-e^{-y}\right)^{-1/2}. \tag{11b}$$

On galaxy scales, $\hat{\nu}_1(y)$ corresponds closely to the simple function $\nu_1(y)$ and $\hat{\nu}_2(y)$ to the standard function $\nu_2(y)$ (Fig. 1). On solar system scales, the simple function predicts deviations from purely Newtonian behavior of one part in 10^8, while $\hat{\nu}_1(10^8)$ deviates by only one part in $\exp(10^8)$. While this is certainly a virtue if we wish to avoid even modest MOND effects in the solar

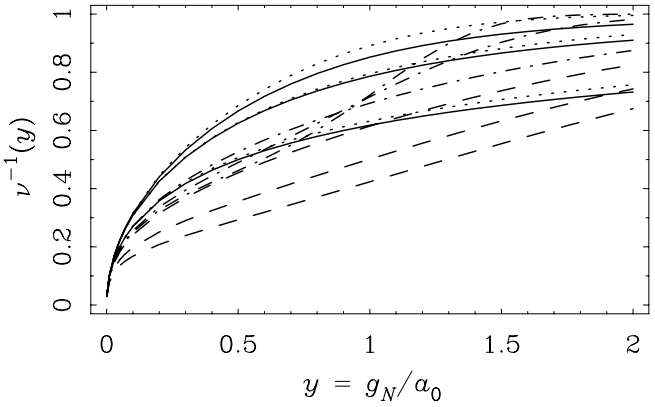

FIG. 1.—MOND interpolation functions with the property $\nu \to 1$ for $y \gg 1$ and $\nu^{-1} \to \sqrt{y}$ for $y \ll 1$. The traditional family ν_n is shown as solid lines with n increasing from bottom to top. The families $\tilde{\nu}_n$ and $\bar{\nu}_n$ are shown as dashed and dash-dotted lines, respectively. For $\tilde{\nu}_n$, increasing n leads to more gradual transitions (lower lines for higher n, opposite the case of the other families). For $\bar{\nu}_n$, the lines cross just shy of $y = 1$, with larger n being the higher lines at $y > 1$. The family $\hat{\nu}_n$ is shown as dotted lines, with increasing amplitude for increasing n. This family is very similar to the traditional family with the same index in the vicinity of $y \approx 1$ relevant to galaxy dynamics, but converges to Newtonian behavior much more rapidly at the large accelerations relevant to solar system dynamics. [*See the electronic edition of the Journal for a color version of this figure.*]

system, one theoretically unpleasant aspect of $\hat{\nu}$ is that its transformation to $\hat{\mu}$ is transcendental.

The interpolation functions given above are shown in Figure 1. While the shapes of ν_n and $\hat{\nu}_n$ are similar for similar n, $\tilde{\nu}_n$ and $\bar{\nu}_n$ are rather different.[1] In particular, they have a rather linear region around $y \approx 1$. What effect this might have on rotation curve fits has not yet been explored in detail, but it may be useful in some historically difficult cases (Milgrom & Sanders 2008). The chief effect of increasing n within a given family seems to be to increase the value of the best-fit mass-to-light ratio. This occurs because there is a more pronounced MOND effect already at $y = 1$ with ν_1 than with ν_2 (for example). Thus, less mass is required to attain the same velocity with lower n.

I do not seek here to identify the optimal version of the many possible interpolation functions. Rather, I simply illustrate the effects of a few representative examples. The results are grossly similar, varying only in details as plausible interpolation functions differ only a little.

3. THE MILKY WAY MASS DISTRIBUTION

To describe the stellar mass distribution of the Milky Way, I adopt the results of the recent Tuorla-Heidelberg study (Flynn et al. 2006). This provides a relation between the bulge mass, disk mass, and scale length of the Milky Way (their Fig. 15) that satisfies both the local surface density and the global luminosity. As the assumed scale length of the disk increases, its central surface density decreases, and the bulge mass increases to maintain the necessary central mass (Table 1).

Following Flynn et al. (2006), I adopt a solar radius $R_0 = 8$ kpc. For the circular velocity I take $\Theta_0 = 219$ km s^{-1} (Reid et al. 1999). The latter is only for reference and does not enter into the models constructed here. The choice of R_0 is relevant as it affects the total scale of the problem. I explore a range of scale lengths R_d at fixed R_0. The details will change for different choices of R_0 since MOND imposes a specific physical scale, and the total mass will scale with R_0. However, the differences over the plausible range of R_0 are not likely to be great compared to the variation due to R_d/R_0.

[1] There is some overlap between families. For example, $\hat{\nu}_1 = \bar{\nu}_{1/2}$ but $\hat{\nu}_2 \neq \bar{\nu}_{3/2}$.

TABLE 1
MILKY WAY MODELS

R_d (kpc)	Σ_0 ($M_\odot$ pc^{-2})	$M_{\rm disk}$ (10^{10} $M_\odot$)	$M_{\rm bulge}$ (10^{10} $M_\odot$)	M_b (10^{10} $M_\odot$)
2.0.....	2133	5.36	0	6.54
2.1.....	1765	4.89	0.09	6.16
2.2.....	1480	4.50	0.40	6.08
2.3.....	1270	4.22	0.67	6.07
2.4.....	1097	3.97	0.91	6.06
2.5.....	960	3.77	1.10	6.05
2.7.....	755	3.46	1.37	6.01
3.0.....	562	3.18	1.66	6.02
3.5.....	383	2.95	1.91	6.04
4.0.....	287	2.89	2.07	6.14

NOTES.—The central surface density Σ_0 is inferred from the scale length–disk mass–bulge mass relation of the Tuorla-Heidelberg model (Flynn et al. 2006). The total baryonic mass $M_b = M_{\rm disk} + M_{\rm bulge} + M_{\rm gas}$ is the sum of all known nonnegligible baryonic components.

The particular model adopted for the baryonic mass distribution of the Milky Way certainly matters. For the appropriate choice of scale length, the Tuorla-Heidelberg model is very similar to the Basel model (Bissantz et al. 2003) employed by Famaey & Binney (2005). However, even small differences are perceptible in MOND. I employ the Tuorla-Heidelberg model here because of its novelty and to enable an exploration of the effects of the scale length. The more important advance, however, is likely the inclusion of the gas distribution (§ 3.3).

3.1. *The Stellar Disk*

The stellar disk is assumed to follow an exponential distribution,

$$\Sigma_\star(R) = \Sigma_0 e^{-R/R_d}. \tag{12}$$

The central surface density Σ_0 is computed from the disk mass of the Tuorla-Heidelberg model for the appropriate choice of scale length (Table 1). The disk is assumed to have a finite thickness with an exponential vertical distribution with $z_d = 300$ pc (Siegel et al. 2002). The distinction between thick and thin disk is relatively unimportant here as most of the mass is in the thin disk. The choice of z_d is relevant only to the detailed computation of V_b; plausible deviations are smaller than the variation in interpolation functions.

I consider scale lengths in the range 2 kpc $\leq R_d \leq$ 4 kpc. At the lower limit of this range, the Tuorla-Heidelberg model has a purely exponential surface density distribution. At the upper limit of this range, the Milky Way disk starts to become rather low surface brightness. The scale length suggested by *COBE L*-band data is 2.5 kpc (Binney et al. 1997), while more recently Gerhard (2002, 2006) has suggested a shorter $R_d = 2.1$ kpc. In varying the scale length, it turns out that MOND prefers a rather short scale length consistent with these estimates, the precise value depending somewhat on the choice of interpolation function and the choice of comparison data.

3.2. *The Bulge*

The distribution of bulge mass follows the triaxial distribution determined by Binney et al. (1997):

$$\rho_{\rm bulge}(b) = \frac{\rho_{\rm bulge,0}}{\eta\zeta b_m^3} \frac{\exp\left[-(b/b_m)^2\right]}{(1 + b/b_0)^{1.8}}, \tag{13}$$

where $b^2 = x^2 + (y/\eta)^2 + (z/\zeta)^2$. They base this profile on fits to the *COBE L*-band data, finding $b_m = 1.9$ kpc, $b_0 = 0.1$ kpc, $\eta = 0.5$, and $\zeta = 0.6$.

In order to compute g_N for the bulge, I neglect the triaxiality and use the sphere that is geometrically equivalent to equation (13). This gives the same run of mass with radius, substituting $r/[(\eta\zeta)^{1/3} b_m]$ for b/b_m and similarly for b/b_0. Then

$$g_{\rm N,\,bulge} = \frac{V^2_{\rm bulge}(R)}{R} = \frac{4\pi G}{R^2}\int_0^R \rho_{\rm bulge}(r) r^2\, dr, \quad (14)$$

which I integrate numerically. The factor $\rho_{\rm bulge,0}$ is scaled to give the correct bulge mass for each choice of scale length (Table 1).

The effects of deviations from this particular bulge model are explored in § 4.1. These details are fairly unimportant here, as they only affect the inner 3 kpc where the motions are noncircular owing to the triaxial distribution of the inner bulge-bar component implied by equation (13). All that matters to the results at $R > 3$ kpc is the total mass enclosed therein.

3.3. *The Gas Disk*

For the gas, I adopt the distribution given by Olling & Merrifield (2001, their Table D1). I include both the molecular and atomic gas components, treating them as being in a negligibly thin disk. I do not include the ionized gas component for consistency with the treatment of other galaxies. Moreover, this is a very small fraction of the total with an estimated surface density ($1.4\, M_\odot\ {\rm pc}^{-2}$) that is only available at the solar radius.

Olling & Merrifield (2001) give the surface densities scaled by R_0. For consistency with the Tuorla-Heidelberg model I fix these numbers to $R_0 = 8$ kpc. The surface densities of H_2 and H I gas are corrected upward by a factor of 1.4 to account for the associated mass in helium and metals. For these assumptions, the gas distribution integrates to a total mass $M_{\rm gas} = 1.18 \times 10^{10}\, M_\odot$. This is slightly more gas mass than inferred by Flynn et al. (2006) from different data, whose total sums to just under $10^{10}\, M_\odot$. This seems like an adequate level of agreement considering the diversity of published opinions.

The gas is usually neglected in mass models of the Milky Way as it is a trace component compared to the stars and dark matter halo. However, the gas is not negligible in MOND. The models considered here have gas mass fractions in the range $f_g = M_{\rm gas}/M_b = 0.19 \pm 0.01$ (Table 1). This is an important component of the total gravitating mass in the absence of dark matter. Effects of the detailed distribution of the gas are reflected in the total rotation curve.

4. THE MILKY WAY ROTATION CURVE

Given the Milky Way mass distribution, MOND predicts the rotation curve. Unlike the case with external galaxies, the mass-to-light ratio is not a fit parameter. The Tuorla-Heidelberg model plus the gas distribution of Olling & Merrifield (2001) specify the mass. The only choices to be made are the scale length and the interpolation function.

Figures 2, 3, and 4 show the results for increasing choices of scale length. In each case, four interpolation functions are illustrated: $\hat{\nu}_1$ and $\hat{\nu}_2$ (these are practically indistinguishable from the simple and standard interpolation functions), and for comparison the functions $\tilde{\nu}_1$ and $\bar{\nu}_1$ newly suggested by Milgrom & Sanders (2008). MOND produces a realistic rotation curve given a mass distribution, especially for the shorter scale lengths preferred by the *COBE* data.

As we increase the scale length to $R_d > 3$ kpc, MOND produces less plausible looking rotation curves. In these cases, the bulge causes a prominent peak in the inner rotation curve. Such a morphology is sometimes seen in early-type spirals (Noordermeer et al. 2007), but the sharp peak in Figure 4 is rather unusual. This aspect is sensitive to the bulge model, and more plausible results are possible (§ 4.1).

Comparison with the observed terminal velocities (Kerr et al. 1986; Malhotra 1995) also favors short scale lengths. The agreement is particularly good for $\hat{\nu}_1$ when $R_d = 2.3$ kpc. The other interpolation functions are hard to distinguish from one another and seem to prefer slightly longer scale lengths $R_d \approx 2.5$ kpc. This result is sensitive to small changes (of order 4%) in the terminal velocity data (§ 5), so stronger statements seem unwarranted.

The Galactic constants can be computed for each model. Table 2 gives the rotation velocity at the solar circle Θ_0 and the Oort constants A and B:

$$A = \frac{1}{2}\left(\frac{\Theta_0}{R_0} - \left.\frac{dV_c}{dR}\right|_{R_0}\right), \quad (15a)$$

$$B = -\frac{1}{2}\left(\frac{\Theta_0}{R_0} + \left.\frac{dV_c}{dR}\right|_{R_0}\right). \quad (15b)$$

The latter depend on the derivative of the rotation curve, which in these models depends somewhat on the extent over which the derivative is measured. That is, there are bumps and wiggles in the rotation curve as a result of the nonsmooth gas distribution (Olling & Merrifield 2001). This causes the derivative to vary in a nontrivial fashion. For specificity, I compute A and B over ± 0.5 kpc around $R_0 = 8$ kpc. One may wonder if this effect has played a role in the various values of the Oort constants that have been derived historically.

The Galactic constants are shown graphically in Figure 5. The measurement of Feast & Whitelock (1997) is most consistent with $\hat{\nu}_1$ for $R_d = 2.1$ kpc. Other interpolation functions and scale lengths are possible, depending on how literally we take the error bars. The function $\hat{\nu}_1$ seems to perform best, with reasonable values of Θ_0, A, and B for $R_d \leq 2.5$ kpc. This interpolation function is very similar to the simple function found by Famaey & Binney (2005) to work best in combination with the Basel model.

The other interpolation functions perform less well, although again one must be cautious as always about the interpretation of astronomical uncertainties. For example, $\tilde{\nu}_1$ gives reasonable Θ_0 up to $R_d = 3$ kpc, but tends to give $A < |B|$ in contradiction to most measurements. Similarly, $\bar{\nu}_1$ gives reasonable B-values, but tends to run low in the other Galactic constants except for the smallest scale lengths. The standard function traditionally used in fitting external galaxies also gives good B-values for all scale lengths, but rather low Θ_0, albeit within the realm of possibility (Olling & Merrifield 1998).

For all interpolation functions, agreement with both the Galactic constants and the terminal velocities steadily deteriorates with increasing scale length. It therefore seems clear that MOND prefers a Milky Way with a short scale length, $R_d \lesssim 2.5$ kpc. There also seems to be a preference for something closer to the simple interpolation function, as found by Famaey & Binney (2005). It seems quite remarkable that given the mass distribution specified by the Tuorla-Heidelberg model for the stars and Olling & Merrifield (2001) for the gas, MOND produces a plausible rotation curve that is consistent with independent terminal velocity data and the observed Galactic constants with no fitting whatsoever.

4.1. *Effects of the Bulge Scale Length*

The model constructed here employs the spherical radial profile that is geometrically equivalent to the observed L-band light distribution of the central bulge-bar component. This results in a rotation curve for this component that is very similar to that of Englmaier & Gerhard (1999), as it should be since it is based on the same data.

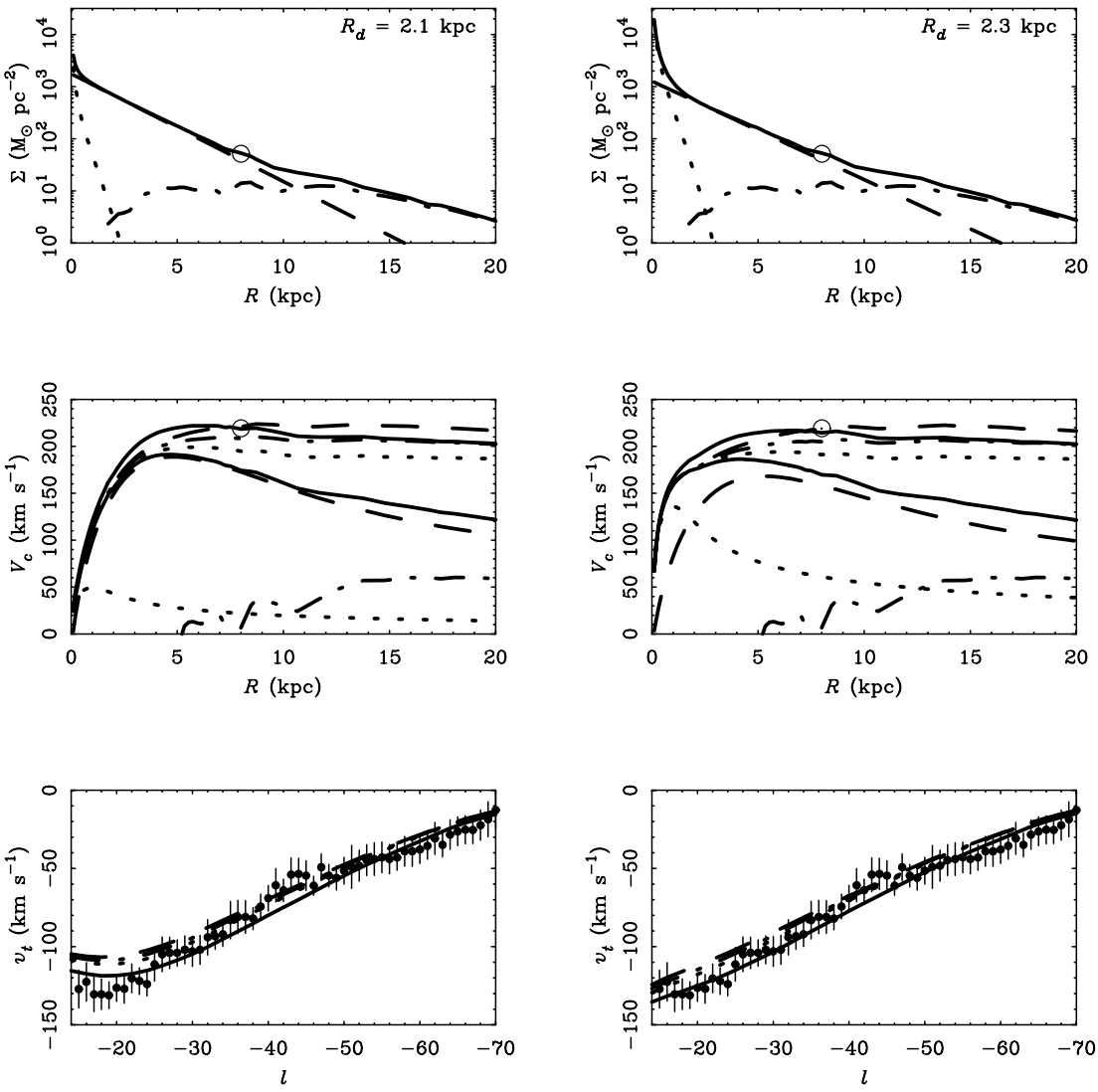

FIG. 2.—Model Milky Ways for assumed disk scale lengths of 2.1 kpc (*left column*) and 2.3 kpc (*right column*). The top panels show the bulge (*dotted line*), stellar disk (*dashed line*), gas (both H_2 and H I; *dash-dotted line*), and total (*solid line*) surface mass distribution. The middle panels shows the Newtonian rotation curve for each of these components, plus the rotation curve predicted by MOND for four choices of interpolation function: $\hat{\nu}_1$ (*solid line*), $\hat{\nu}_2$ (*dotted line*), $\tilde{\nu}_1$ (*dashed line*), and $\bar{\nu}_1$ (*dash-dotted line*). The solar value $\Theta_0 = 219$ km s^{-1} at $R_0 = 8$ kpc is marked by the open circle. In the bottom panels, the MOND predictions are compared to the terminal velocity data (Kerr et al. 1986; Malhotra 1995). [*See the electronic edition of the Journal for a color version of this figure.*]

However, it rises more steeply than that of Bissantz et al. (2003) owing to the different treatment of spiral arms there. The latter appears consistent with the same mass profile with a larger scale length.

Figure 6 shows the effect of varying the bulge scale length. Two cases are illustrated: that described in § 3.2, and one with the same distribution but a longer scale length. The former uses the geometric scaling $(\eta\zeta)^{1/3}$ while the latter uses no scaling. In effect, r is directly substituted for b in equation (13) with no geometric correction to b_m and b_0. This latter case gives a softer bulge more consistent with Bissantz et al. (2003).

The shape of the inner rotation curve is affected by the choice of scale length, with a much steeper rate of rise for shorter length scales. The longer scale length bulge model results in less of a peak and produces morphologically reasonable rotation curves for disks of all scale lengths. Even the $R_d = 4$ kpc case appears plausible, although the maximum rotation velocity barely exceeds 200 km s^{-1}.

The details of the bulge model make no difference at $R > 3$ kpc. Since the orbits within this radius are apparently noncircular thanks to the triaxiality of the central component, we make no attempt to fit this region. To do so would require detailed MONDian simulations that are well beyond the scope of this paper. What matters here is basically just the mass enclosed within 3 kpc, which is constrained by a great deal of data (Gerhard 2006).

4.2. *The Outer Rotation Curve*

The rotation curve of the Galaxy beyond the solar circle is rather more difficult to constrain than that within it (e.g., Binney & Dehnen 1997; Frinchaboy 2006). MOND predicts the rotation curve for the given mass distribution quite far out, to where the external field from other galaxies starts to become important (Famaey et a. 2007; Wu et al. 2008). Recently, Xue et al. (2008) estimated the rotation curve of the Milky Way out to 55 kpc from blue horizontal branch stars found in the Sloan Digital Sky Survey (SDSS). Figure 7 shows the extrapolation out to these radii.

MOND was constructed to give asymptotically flat rotation curves. However, the detailed shape of the rotation curve depends on the details of the mass distribution. The rotation curve may rise or fall toward the asymptotic value, and may not become flat until quite far out. For our Galaxy, the rotation speed predicted by MOND declines gradually from the solar value to

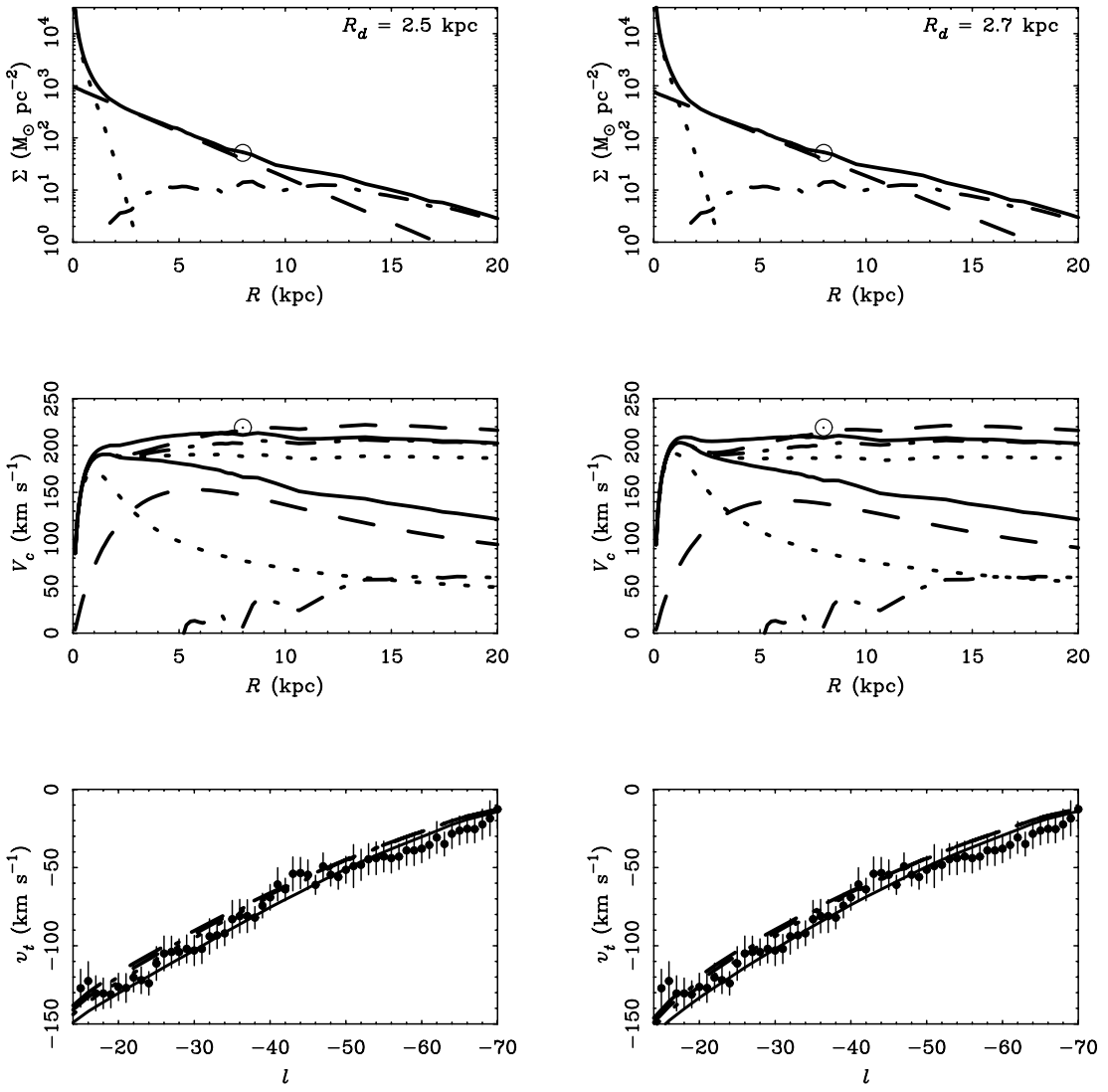

FIG. 3.—Same as Fig. 2, but for $R_d = 2.5$ and 2.7 kpc. [*See the electronic edition of the Journal for a color version of this figure.*]

$\sim$185 km s^{-1} at $\sim$50 kpc, asymptoting to $\sim$180 km s^{-1}. Such a gradually declining rotation curve helps to reconcile the apparent (albeit minor) discrepancy between the Milky Way and the Tully-Fisher relation (McGaugh 2005, Flynn et al. 2006; Hammer et al. 2007): Θ_0 is a bit larger than V_f. More importantly, this prediction appears to be consistent with the SDSS data.

Xue et al. (2008) employ ΛCDM simulations to aid in the interpretation of the SDSS data. This is obviously inappropriate for a MONDian analysis. Indeed, one wonders if it is appropriate at all given the difficulties ΛCDM models persistently face on galaxy scales (e.g., Kuzio de Naray et al. 2006; McGaugh et al. 2007). The Milky Way itself is problematic in this regard (Binney & Evans 2001). The baryon distributions of neither the Tuorla-Heidelberg model nor the Basel model tolerate the expected cusp in the dark matter halo. As with other bright spirals, the baryons account for too much of the rotation curve budget at small radii. Hopefully the result of Xue et al. (2008) is dominated by the data and would not change greatly with a different analysis.

5. THE INVERSE PROBLEM: SURFACE DENSITIES FROM VELOCITIES

The Tuorla-Heidelberg model gives very useful constraints on the mass distribution of the Milky Way, but it is still couched in terms of a smooth exponential disk. Real galaxies deviate somewhat from pure exponentials, and these bumps and wiggles in the surface brightness are reflected in the rotation curve (Renzo's rule: Sancisi 2004; McGaugh 2004). One wonders if this might also be the case for the Milky Way.

Recently, very high quality estimates of the terminal velocities in the fourth quadrant have become available (Luna et al. 2006; McClure-Griffiths & Dickey 2007). These suggest the possibility of reversing the exercise above, and inferring the surface density distribution of the Milky Way from these data. Note that equation (3) can be inverted to obtain the baryonic rotation curve from the observed terminal velocity curve: $V_b = V_c/\sqrt{\nu}$. Then the inversion to surface density becomes a purely Newtonian problem. In principle, this can be accomplished by employing equation (2-174) of Binney & Tremaine (1987):

$$\Sigma(R) = \frac{1}{\pi^2 G}\left[\frac{1}{R}\int_0^R \frac{d^2}{dR}\,K\left(\frac{u}{R}\right)du + \int_R^\infty \frac{d^2}{dR}\,K\left(\frac{R}{u}\right)\frac{du}{u}\right]. \quad (16)$$

Note that this procedure should work even in the context of dark matter. If MOND is not correct as a theory, the interpolation

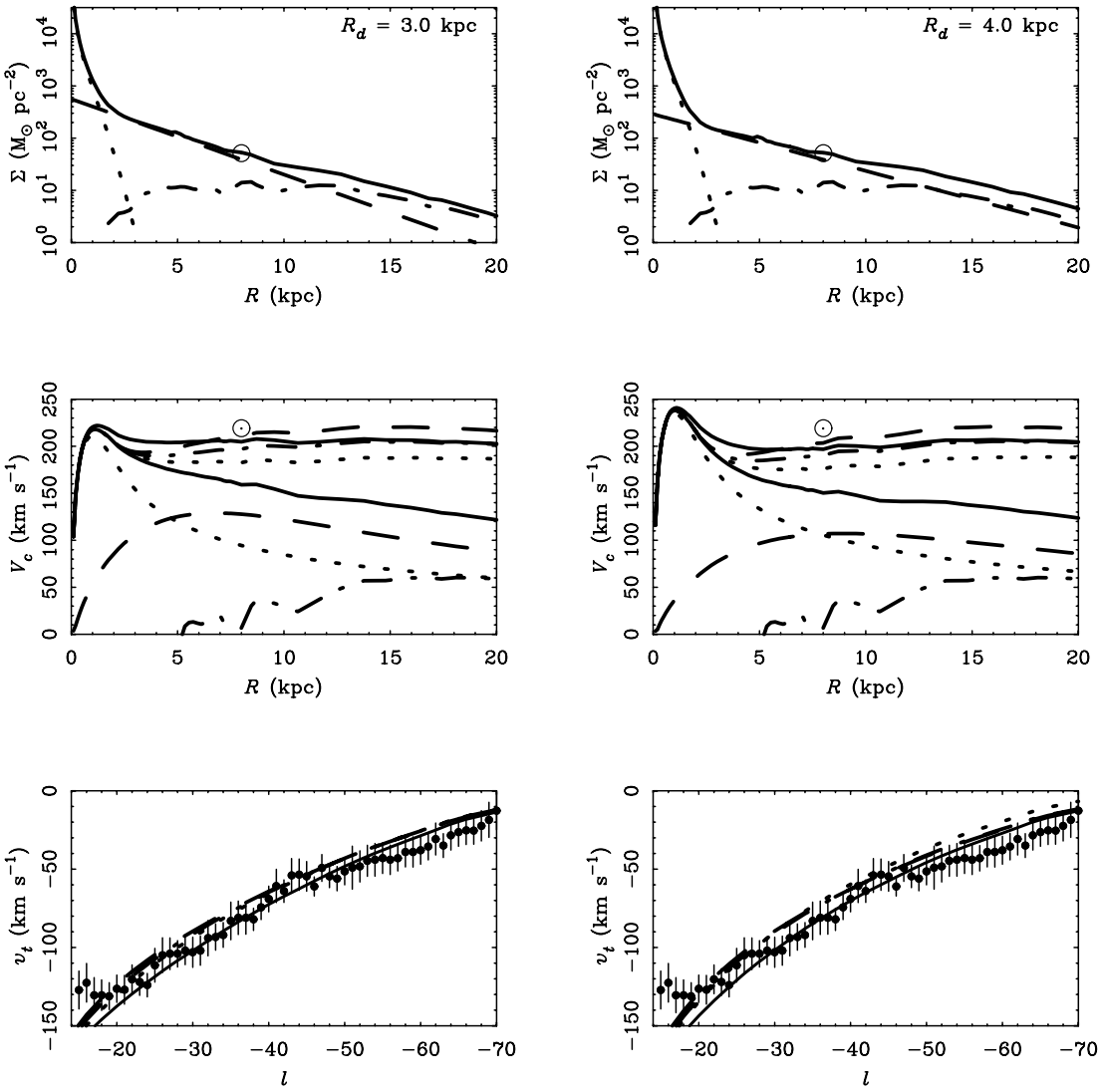

FIG. 4.—Same as Fig. 2, but for $R_d = 3$ and 4 kpc. [*See the electronic edition of the Journal for a color version of this figure.*]

function still provides an empirical link between V_b and V_c (McGaugh 2004). In practice, however, application of equation (16) is fraught with peril. The elliptic integral K peaks very sharply as $u \to R$. Moreover, one must know the derivative of the square of the rotation curve very well. Even though the new data are very good, there are many abrupt changes in the derivative. Moreover, the data extend only over a finite range of radii, while the integral must be completed everywhere.

A more practical approach is one of iterative trial and error, computing g_N from a trial mass distribution in the usual way, then

TABLE 2
GALACTIC CONSTANTS

	$\hat{\nu}_1$			$\tilde{\nu}_1$			$\bar{\nu}_1$			$\hat{\nu}_2$		
R_d	Θ_0	A	B	Θ_0	A	B	Θ_0	A	B	Θ_0	A	B
2.0	225	15.2	−12.8	226	13.3	−14.8	214	13.5	−13.2	201	13.7	−11.3
2.1	218	14.3	−12.8	221	12.7	−14.8	208	12.8	−13.2	195	12.8	−11.4
2.2	215	13.9	−12.9	218	12.4	−14.8	206	12.4	−13.2	192	12.4	−11.5
2.3	214	13.7	−13.0	218	12.3	−14.9	205	12.2	−13.3	191	12.2	−11.6
2.4	212	13.3	−13.1	216	12.0	−14.9	203	11.9	−13.3	189	11.8	−11.7
2.5	211	13.1	−13.1	215	11.9	−14.9	202	11.8	−13.4	188	11.7	−11.7
2.7	208	12.7	−13.2	213	11.6	−14.9	199	11.4	−13.4	185	11.3	−11.8
3.0	205	12.2	−13.3	210	11.3	−14.9	197	11.0	−13.5	183	10.8	−11.9
3.5	200	11.6	−13.3	206	10.8	−14.8	193	10.5	−13.5	179	10.3	−12.0
4.0	197	11.3	−13.2	204	10.6	−14.7	190	10.3	−13.4	176	10.0	−11.9

NOTES.—Galactic constants as predicted by each interpolation function ν for each choice of disk scale length. Galactic units are used: R_d is in kiloparsecs, Θ_0 is in kilometers per second, and A and B are in kilometers per second per kiloparsec.

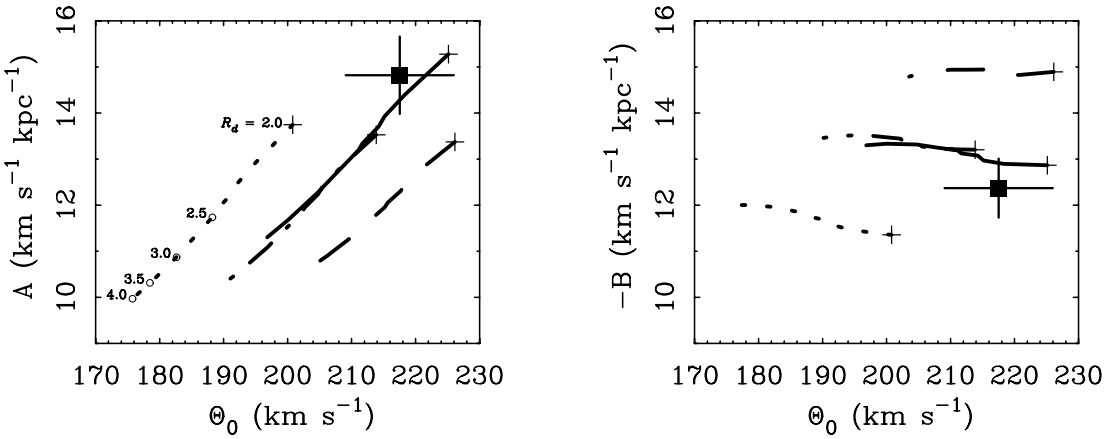

FIG. 5.— Oort A and B constants for the various models as a function of $\Theta_0 = V_c(R_0)$. All models assume $R_0 = 8$ kpc; see Table 2 for the derived values of the other Galactic constants. A cross marks the model with the shortest (2 kpc) scale length for each choice of interpolation function (*lines as in Fig. 2*); progressively larger R_d proceed along each line as illustrated by the open circles at left. The data points represent the observed values determined by Feast & Whitelock (1997). These give $\Theta_0 = (A - B)R_0 = 217.5$ km s^{-1}, very close to the 219 km s^{-1} obtained from the proper motion of Sgr A* (Reid et al. 1999). The precise values of A and B in the models depend somewhat on the range over which they are measured, as the bumps and wiggles in the gas distribution perturb the local value of the gradient in the rotation curve (Olling & Merrifield 2001). [*See the electronic edition of the Journal for a color version of this figure.*]

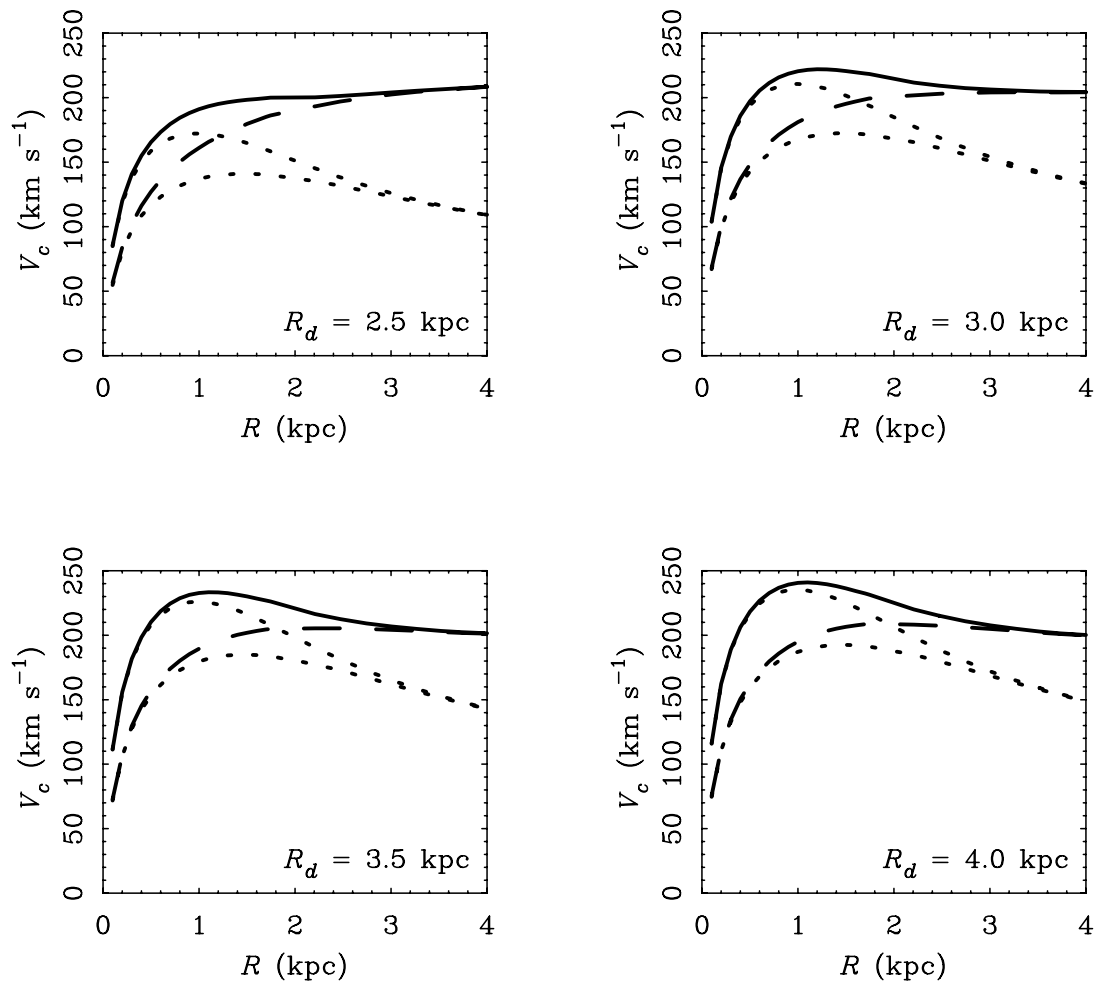

FIG. 6.— Effect of the bulge model. In each of the illustrated cases, the shape of the bulge mass profile is identical. The total mass of the bulge changes with the scale length of the disk according to the prescription of the Tuorla-Heidelberg model (Flynn et al. 2006). In each panel, the two bulge models (*dotted lines*) differ only in their effective scale length. The upper pair of lines follow from the bulge model computed in § 3.2 and is similar to the model of Englmaier & Gerhard (1999). The lower pair of lines makes no geometric correction for the triaxial shape of the bulge, yet corresponds more closely to the model of Bissantz et al. (2003). Differences between bulge models are imperceptible outside of 3 kpc. [*See the electronic edition of the Journal for a color version of this figure.*]

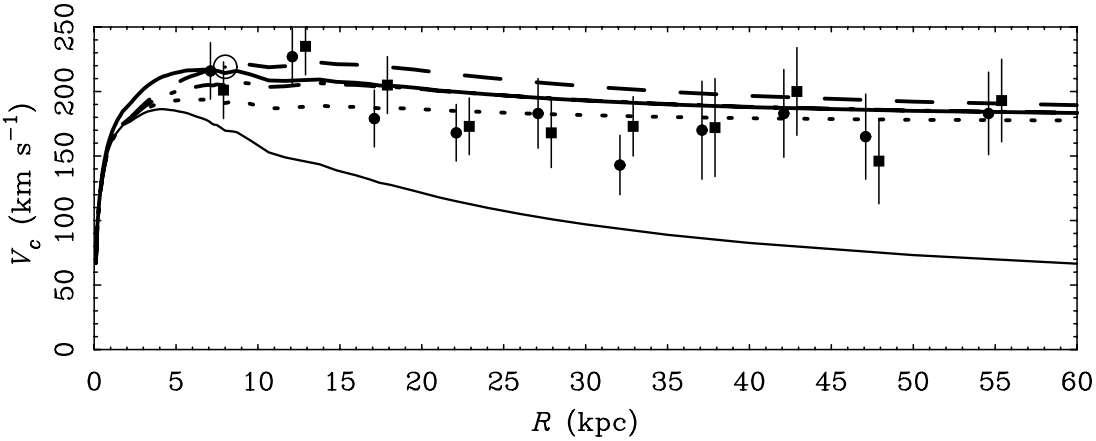

FIG. 7.—Outer rotation curve predicted by MOND for the Milky Way compared to the two realizations of the blue horizontal branch stars in the SDSS data reported by Xue et al. (2008). The data points from the two realizations have been offset slightly from each other in radius for clarity; the lines are as in Fig. 2. The specific case illustrated has $R_d = 2.3$ kpc, but the rotation curve beyond 15 kpc is not sensitive to this choice. While the data clearly exceed the Newtonian expectation (declining curve), they are consistent with MOND. [*See the electronic edition of the Journal for a color version of this figure.*]

tweaking it to bring it closer to the data. The new terminal velocities, which are consistent in shape with the older data, are $\sim$8 km s^{-1} higher in amplitude. This appears largely to result from the method by which the maximum line-of-sight velocity is estimated (see extensive discussion in McClure-Griffiths & Dickey 2007). While this hardly seems like a large offset ($\sim$4%), it is quite noticeable in MOND. It implies higher surface densities, albeit well within the uncertainties of the Tuorla-Heidelberg model. Given the current interarm location of the Sun, it might even be desirable to have the azimuthally averaged surface density at the solar radius be somewhat higher than the local column.

The case of $\hat{\nu}_1$ with $R_d = 2$ kpc is the smooth case that comes closest to matching the data of Luna et al. (2006) and McClure-Griffiths & Dickey (2007). Starting from this initial guess, I perturb the surface density profile by manually adjusting the surface densities in the range necessary to affect the terminal velocity data. To be specific, I match the data of Luna et al. (2006) in the range 3 kpc $\leq R \leq$ 7.8 kpc. Velocities inside 3 kpc are not fit since the motions there are thought to be noncircular, and the details of the choice of bulge model begin to matter (§ 4.1). For simplicity I assume that the inner distribution is purely exponential, but this does not matter so long as the enclosed mass remains the same. One could just as well imagine a Galaxy with an inner bulge plus Freeman type II profile that sums to the same mass.

The procedure is to adjust the surface density profile manually, estimating the amount to adjust by the desired $\Delta V_c^2 R$. I then use the routine ROTMOD in GIPSY (van der Hulst et al. 1992) to compute V_b for the perturbed surface density distribution. I compare $V_c = \hat{\nu}_1^{1/2}(y)V_b$ to the data, and repeat the procedure. Although tedious, this procedure can be made to converge with sufficient patience. That is, it is possible to obtain a model that matches the detailed shape of the terminal velocity data.

The result of this procedure is presented in Figure 8. Note that in order to affect the velocity at 3 kpc, it is necessary to start adjusting the surface density somewhere inside of that. The inferred stellar surface densities and corresponding velocities are given in Table 3. Outside of this range, the stellar density remains that of a purely exponential disk. The gas is assumed to follow the distribution of Olling & Merrifield (2001); only the stellar disk has been adjusted. The total mass is 2% higher than the initial pure exponential disk: $M_{\rm disk} = 5.48 \times 10^{10}\, M_\odot$.

We should be careful not to overinterpret the result. I have only fit one choice of interpolation function ($\hat{\nu}_1$); other choices would give somewhat different results. Moreover, the assumption of circular motion is implicit; streaming motions along the spiral arms are likely to be present at some level. Indeed, Luna et al. (2006) give $V_c(R = 7.8\ {\rm kpc}) = 233.6$ km s^{-1}. This is difficult to reconcile with $\Theta_0(R_0 = 8.0\ {\rm kpc}) = 219$ km s^{-1} (Reid et al. 1999) with purely circular motion in any type of model. Variations of this sort are at least conceivable in MOND (Fig. 8), but probably reflect a real difference between the first and fourth quadrants. Hence, I have made no attempt to force a fit to the solar value.

The Oort constants of this model are fairly reasonable: $A = 15.9$ km s^{-1} kpc^{-1} and $B = -13.0$ km s^{-1} kpc^{-1}. The value of A may seem a bit high, but note that since the rotation velocity is inferred to be higher than the solar value, $A - B$ must also be higher. This is in the data. The model fits the detailed terminal velocity curve as far as it is reported (up to $R = 7.8$ kpc), so these are in effect the measured values of the Oort constants in the fourth quadrant. There is only a modest model-dependent extrapolation to the solar radius. Barring systematic errors in the data or sharp features in the rotation curve near the solar radius, the uncertainty in these estimates is <1 km s^{-1} kpc^{-1}.

Indeed, it is instructive that this exercise can be successfully done at all. The inferred surface density has the sorts of bumps and wiggles commonly observed in the azimuthally averaged surface brightness profiles of spiral galaxies. These correspond to the bumps and wiggles in the rotation curve, as they must in MOND, and as they are observed to do in general (Renzo's rule). This correspondence follows in the dark matter picture only if disks are dynamically important. This is hard to arrange with the cuspy halos obtained in CDM simulations (e.g., Navarro et al. 1997) as these place too much dark mass at small radii. Low surface brightness (LSB) disks cannot have dynamically significant mass in the dark matter picture (de Blok & McGaugh 1997), yet still obey the correspondence of bumps and wiggles encapsulated by Renzo's rule (e.g., Broeils 1992). This occurs naturally in MOND, the a priori predictions of which (Milgrom 1983b) are realized in LSB galaxies (Milgrom & Braun 1988; McGaugh & de Blok 1998).

The specific pattern of bumps and wiggles seen in Figure 8 is in principle testable by star count analyses. In particular, it is tempting to associate the dip in surface density at $\sim$5 kpc and the subsequent shelf with a ring or spiral arms, perhaps emanating from the end of the long ($\sim$4.5 kpc) bar (Cabrera-Lavers et al. 2007)—a morphology frequently seen in other galaxies and naturally reproduced in MOND simulations (Tiret & Combes 2007).

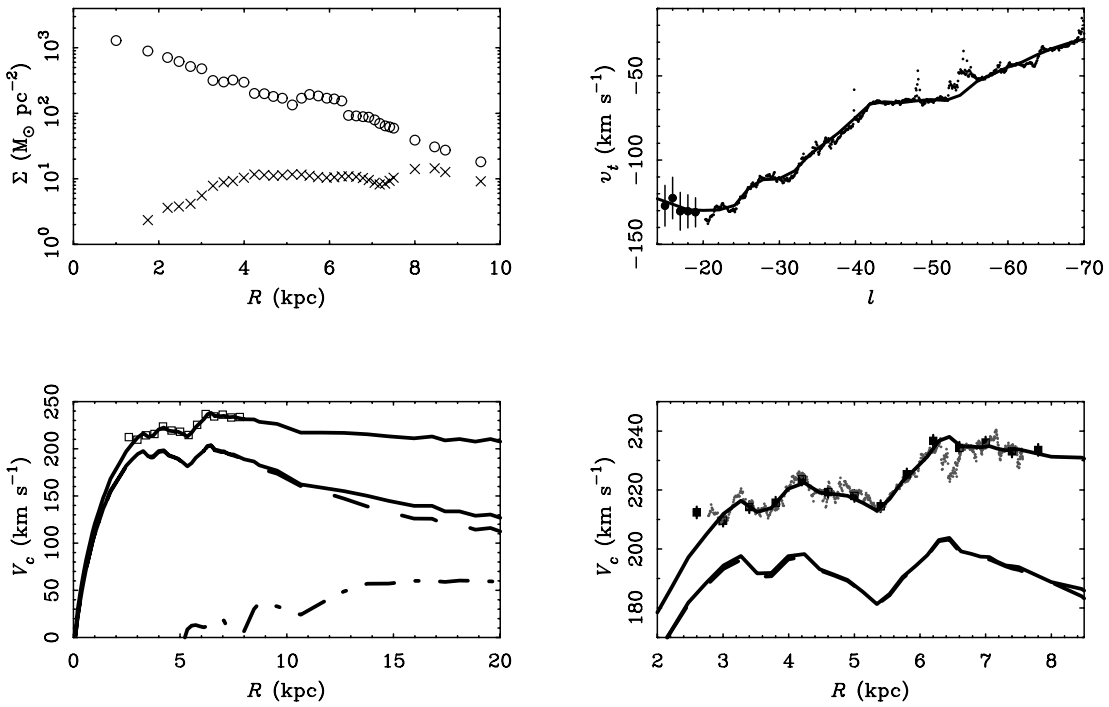

FIG. 8.—Milky Way stellar surface density (*top left, circles*) inferred from the terminal velocity data assuming $\hat{v}_1$ and the illustrated gas surface densities (*crosses*). The terminal velocities of McClure-Griffiths & Dickey (2007) are shown at top right together with the MOND model fit to the data of Luna et al. (2006). The latter are shown as squares in the bottom panels. The total and component rotation curves are shown as in Fig. 2 at bottom left. At bottom right is a close-up of the fit region with both terminal velocity data sets. The bumps and wiggles in the velocity data can be reproduced, giving features similar to those seen in external galaxies in both $\Sigma(R)$ and $V_c(R)$. [*See the electronic edition of the Journal for a color version of this figure*.]

TABLE 3
INFERRED SURFACE DENSITIES

R (kpc)	$\Sigma_\star$ ($M_\odot$ pc^{-2})	V_c (km s^{-1})
2.47	620	197
2.74	520	204
3.01	480	211
3.27	318	216
3.52	300	212
3.74	323	213
3.99	299	220
4.24	200	222
4.47	199	219
4.69	180	218
4.90	170	218
5.18	135	215
5.34	170	213
5.54	195	216
5.74	185	223
5.94	170	227
6.11	165	231
6.29	155	236
6.45	93	238
6.62	91	234
6.78	89	234
6.92	87	234
7.06	79	234
7.18	70	234
7.30	65	233
7.41	62	233
7.50	59	233

NOTE.—Stellar surface densities outside this range follow an exponential distribution with $R_d = 2.0$ kpc and $\Sigma_0 = 2133\ M_\odot$ pc^{-2}.

Again however, the details of star counts will depend on the choice of interpolation function and the level of noncircular motions. Indeed, even for a given interpolation function and purely circular motion, the result at this level of detail depends on whether we use the modified gravity of Bekenstein & Milgrom (1984; eq. [2]) or modified inertia (eq. [1]). I have implicitly assumed the latter here.

Another intriguing thing to note is that a fit to the surface densities in Table 3 gives $R_d = 2.4$ kpc even though the base model has $R_d = 2.0$ kpc. This type of variation in R_d with the fit radial range is commonly found in external galaxies, and may go some way to explaining the variation in reported scale lengths for the Milky Way (Sackett 1997). Clearly MOND prefers a compact Milky Way, consistent with the *COBE* data (Binney et al. 1997; Drimmel & Spergel 2001) and the rather high observed microlensing optical depth (Popowski et al. 2005) that requires that baryonic mass dominate within the solar circle (Binney & Evans 2001; Bissantz et al. 2004).

A related test of MOND in the Milky Way is provided by the vertical support of the stellar and gas disks. In the outskirts of the Galaxy, the baryonic components should flare substantially as the effective mass scale height comes to be dominated by the quasi-spherical dark matter halo. In contrast, the potential remains disk-like close to the plane in MOND. The net effect is that MONDian disks will be somewhat thinner, all other things being equal.

Recently, Sánchez-Salcedo et al. (2008) have analyzed the thickness of the gas layer of the Milky Way in the context of MOND. They find that MONDian self-gravity of the disk provides a plausible explanation of the thickness and flaring of the gas layer. Milgrom (2008) points out that the form of the interpolation function as well as the mass model matters to the details of the support of the gas layer. It also seems possible that magnetic field support may be nonnegligible, so a perfect fit might be difficult to obtain.

In comparison, it is necessary to invoke a massive ($>10^{11}\,M_\odot$) ring-like dark matter component in addition to the traditional quasi-spherical halo in order to explain the gas thickness in conventional terms (Kalberla et al. 2007).

For stars, MOND will support a higher vertical velocity dispersion at a given disk thickness. This effect in the Milky Way is rather subtle until large radii (Nipoti et al. 2007), but might conceivably be detectable with *Gaia*. The large velocity dispersions of planetary nebulae at large radii in face-on spirals might be an indication of such an effect (Herrmann & Ciardullo 2005).

6. CONCLUSIONS

By treating the Milky Way as we would an external galaxy, it is possible to obtain the rotation curve from the surface density with MOND. There is no freedom to adjust the mass-to-light ratio as in external galaxies. The result is satisfactory provided the scale length of the Milky Way is relatively short (2–2.5 kpc), as implied by the *COBE* data (Binney et al. 1997; Gerhard 2002, 2006). It is also possible to invert the procedure and derive a plausible detailed surface density distribution from the observed terminal velocity curve.

The major conclusions of this work are as follows.

1. Given the observed stellar and gas mass distribution of the Milky Way, MOND naturally produces a plausible rotation curve that is consistent with the relevant dynamical data. This follows with no fitting.

2. MOND prefers Milky Way models with relatively short ($2.0\,\mathrm{kpc} \lesssim R_d \lesssim 2.5$ kpc) scale lengths. In this range, rotation curves that look familiar from the study of external galaxies are produced. As the scale length is increased beyond this range, the morphology of the resulting rotation curve becomes less realistic, and the match to kinematic data becomes worse.

3. The Milky Way data seem to prefer an interpolation function close to the simple form, in agreement with the findings of Famaey & Binney (2005). The precise form that is preferred depends on the details of the adopted Milky Way model, so it is unclear how definitive a statement can be made.

4. An interpolation function that shares the virtues of the simple function on galaxy scales without having as large an impact on solar system dynamics is $\hat{\nu}_1^{-1}(y) = 1 - \exp(-\sqrt{y})$. Other forms are possible. Empirical calibration of this function is desirable, even in the context of dark matter, since it encapsulates the coupling between mass and light.

5. It is possible to recover the detailed surface mass density of the Milky Way from the observed terminal velocities. The result is a Galaxy with bumps and wiggles in both its luminosity profile and rotation curve that are reminiscent of those frequently observed in external galaxies.

6. A prominent feature among the bumps and wiggles is a shelf around ~5.5 kpc. This might correspond to a ring or spiral arms, perhaps extending from the ends of the long bar. Fitting the profile including the bumps and wiggles gives $R_d = 2.4$ kpc even though the mass scale length is 2 kpc.

7. The Oort constants in the fourth quadrant are estimated to be $A = 15.9\ \mathrm{km\ s^{-1}\ kpc^{-1}}$ and $B = -13.0\ \mathrm{km\ s^{-1}\ kpc^{-1}}$.

It is hard to imagine that all this could follow from a formula devoid of physical meaning.

The author is grateful for conversations with Moti Milgrom, Garry Angus, and Benoit Famaey, and for constructive input from the referee. The work of S. S. M is supported in part by NSF grant AST 05-05956.

REFERENCES

Anderson, J. D., Laing, P. A., Lau, E. L., Liu, A. S., Nieto, M. M., & Turyshev, S. G. 1998, Phys. Rev. Lett., 81, 2858
Angus, G. W., Famaey, B., & Buote, D. A. 2008, MNRAS, 387, 1470
Angus, G. W., & McGaugh, S. S. 2008, MNRAS, 383, 417
Angus, G. W., Shan, H. Y., Zhao, H. S., & Famaey, B. 2007, ApJ, 654, L13
Begeman, K. G., Broeils, A. H., & Sanders, R. H. 1991, MNRAS, 249, 523
Bekenstein, J. D. 2004, Phys. Rev. D, 70, 083509
———. 2006, Contemp. Phys., 47, 387
Bekenstein, J. D., & Milgrom, M. 1984, ApJ, 286, 7
Binney, J., & Dehnen, W. 1997, MNRAS, 287, L5
Binney, J., & Evans, N. W. 2001, MNRAS, 327, L27
Binney, J., Gerhard, O., & Spergel, D. 1997, MNRAS, 288, 365
Binney, J., & Tremaine, S. 1987, Galactic Dynamics (Princeton: Princeton Univ. Press)
Bissantz, N., Debattista, V. P., & Gerhard, O. 2004, ApJ, 601, L155
Bissantz, N., Englmaier, P., & Gerhard, O. 2003, MNRAS, 340, 949
Bissantz, N., & Gerhard, O. 2002, MNRAS, 330, 591
Bottema, R., Pestaña, J. L. G., Rothberg, B., & Sanders, R. H. 2002, A&A, 393, 453
Bournaud, F., et al. 2007, Science, 316, 1166
Brada, R., & Milgrom, M. 1995, MNRAS, 276, 453
Broadhurst, T., & Barkana, R. 2008, MNRAS, submitted (arXiv:0801.1875)
Broeils, A. H. 1992, A&A, 256, 19
Cabrera-Lavers, A., Hammersley, P. L., González-Fernández, C., López-Corredoira, M., Garzón, F., & Mahoney, T. J. 2007, A&A, 465, 825
Clowe, D., Bradač, M., Gonzalaz, A. H., Markevitch, M., Randall, S. W., Jones, C., & Zaritsky, D. 2006, ApJ, 648, L109
de Blok, W. J. G., & McGaugh, S. S. 1997, MNRAS, 290, 533
———. 1998, ApJ, 508, 132
Drimmel, R., & Spergel, D. N. 2001, ApJ, 556, 181
Englmaier, P., & Gerhard, O. 1999, MNRAS, 304, 512
Famaey, B., & Binney, J. 2005, MNRAS, 363, 603
Famaey, B., Bruneton, J.-P., & Zhao, H. 2007, MNRAS, 377, L79
Feast, M., & Whitelock, P. 1997, MNRAS, 291, 683
Felten, J. E. 1984, ApJ, 286, 3
Flynn, C., Holmberg, J., Portinari, L., Fuchs, B., & Jahreiß, H. 2006, MNRAS, 372, 1149
Frinchaboy, P. M. I. 2006, Ph.D. thesis, Univ. Virginia
Gentile, G., Famaey, B., Combes, F., Kroupa, P., Zhao, H. S., & Tiret, O. 2007, A&A, 472, L25
Gerhard, O. 2002, Space Sci. Rev., 100, 129
———. 2006, EAS Publ. Ser., 20, 89
Hammer, F., Puech, M., Chemin, L., Flores, H., & Lehnert, M. D. 2007, ApJ, 662, 322
Hayashi, E., & White, S. D. M. 2006, MNRAS, 370, L38
Herrmann, K. A., & Ciardullo, R. 2005, in AIP Conf. Proc. 804, Planetary Nebulae as Astronomical Tools, ed. R. Szczerba, G. Stasinska, & S. K. Górny (Melville: AIP), 341
Iorio, L. 2008, J. Gravitational Phys., 2, 26
Jee, M. J., et al. 2007, ApJ, 661, 728
Kalberla, P. M. W., Dedes, L., Kerp, J., & Haud, U. 2007, A&A, 469, 511
Kerr, F. J., Bowers, P. F., Jackson, P. D., & Kerr, M. 1986, A&AS, 66, 373
Kuzio de Naray, R., McGaugh, S. S., de Blok, W. J. G., & Bosma, A. 2006, ApJS, 165, 461
Luna, A., Bronfman, L., Carrasco, L., & May, J. 2006, ApJ, 641, 938
Malhotra, S. 1995, ApJ, 448, 138
McCarthy, I. G., Bower, R. G., & Balogh, M. L. 2007, MNRAS, 377, 1457
McClure-Griffiths, N. M., & Dickey, J. M. 2007, ApJ, 671, 427
McCulloch, M. E. 2007, MNRAS, 376, 338
McGaugh, S. S. 2004, ApJ, 609, 652
———. 2005, ApJ, 632, 859
———. 2006, preprint (astro-ph/0606351)
McGaugh, S. S., & de Blok, W. J. G. 1998, ApJ, 499, 66
McGaugh, S. S., de Blok, W. J. G., Schombert, J. S., Kuzio de Naray, R., & Kim, J. H. 2007, ApJ, 659, 149
Milgrom, M. 1983a, ApJ, 270, 365
———. 1983b, ApJ, 270, 371
———. 1983c, ApJ, 270, 384
———. 1994, Ann. Phys., 229, 384
———. 1999, Phys. Lett. A, 253, 273

Milgrom, M. 2006, EAS Publ. Ser., 20, 217
———. 2007, ApJ, 667, L45
———. 2008, preprint (arXiv:0801.3133)
Milgrom, M., & Braun, E. 1988, ApJ, 334, 130
Milgrom, M., & Sanders, R. H. 2008, ApJ, 678, 131
Milosavljević, M., Koda, J., Nagai, D., Nakar, E., & Shapiro, P. R. 2007, ApJ, 661, L131
Navarro, J. F., Frenk, C. S., & White, S. D. M. 1997, ApJ, 490, 493
Nipoti, C., Londrillo, P., Zhao, H. S., & Ciotti, L. 2007, MNRAS, 379, 597
Noordermeer, E., van der Hulst, J. M., Sancisi, R., Swaters, R. S., & van Albada, T. S. 2007, MNRAS, 376, 1513
Nusser, A. 2008, MNRAS, 384, 343
Olling, R. P., & Merrifield, M. R. 1998, MNRAS, 297, 943
———. 2001, MNRAS, 326, 164
Pointecouteau, E., & Silk, J. 2005, MNRAS, 364, 654
Popowski, P., et al. 2005, ApJ, 631, 879
Reid, M. J., Readhead, A. C. S., Vermeulen, R. C., & Treuhaft, R. N. 1999, ApJ, 524, 816
Sackett, P. D. 1997, ApJ, 483, 103
Sánchez-Salcedo, F. J., Saha, K., & Narayan, C. A. 2008, MNRAS, 385, 1585
Sancisi, R. 2004, in IAU Symp. 220, Dark Matter in Galaxies, ed. S. D. Ryder et al. (San Francisco: ASP), 233
Sanders, R. H. 1996, ApJ, 473, 117
———. 2003, MNRAS, 342, 901
———. 2005, MNRAS, 363, 459
Sanders, R. H., & McGaugh, S. S. 2002, ARA&A, 40, 263
Sanders, R. H., & Noordermeer, E. 2007, MNRAS, 379, 702
Sanders, R. H., & Verheijen, M. A. W. 1998, ApJ, 503, 97
Sereno, M., & Jetzer, Ph. 2006, MNRAS, 371, 626
Siegel, M. H., Majewski, S. R., Reid, I. N., & Thompson, I. B. 2002, ApJ, 578, 151
Springel, V., & Farrar, G. R. 2007, MNRAS, 380, 911
Tiret, O., & Combes, F. 2007, A&A, 464, 517
van der Hulst, J. M., Terlouw, J. P., Begeman, K. G., Zwitser, W., & Roelfsema, P. R. 1992, in ASP Conf. Ser. 25, Astronomical Data Analysis Software and Systems I, ed. D. M. Worrall, C. Biemesderfer, & J. Barnes (San Francisco: ASP), 131
Wallin, J. F., Dixon, D. S., & Page, G. L. 2007, ApJ, 666, 1296
Widrow, L. M., Pym, B., & Dubinski, J. 2008, ApJ, 679, 1239
Wu, X., Famaey, B., Gentile, G., Perets, H., & Zhao, H. 2008, MNRAS, 386, 2199
Xue, X.-X., et al. 2008, ApJ, in press (arXiv:0801.1232)
Zhao, H.-S., & Famaey, B. 2006, ApJ, 638, L9